Journal of Neonatal Surgery
ISSN(Online): 2226-0439
Vol. 14, Issue 32s (2025)
https://www.jneonatalsurg.com

OPEN ACCESS

Normative Measurement of Ocular Muscle Using Computed Tomography

Unnati Pant[1*], Rashmi Pandey[2]

[*1] M.Sc. Research fellow, Department of Radiological Imaging Techniques, College of Paramedical Sciences, Teerthanker Mahaveer University, Moradabad, Uttar Pradesh, India, 244001.

[2]Assistant Professor, Department of Radiological and Imaging Techniques, College of Paramedical Sciences, Teerthanker Mahaveer University, Moradabad, Uttar Pradesh, India, 244001.

***Corresponding author:**

Unnati pant

M.Sc. Research fellow, Department of Radiological Imaging Techniques, College of Paramedical Sciences, Teerthanker Mahaveer University, Moradabad, Uttar Pradesh, India, 244001.

Cite this paper as: Unnati Pant, Rashmi Pandey, (2025) Normative Measurement of Ocular Muscle Using Computed Tomography. *Journal of Neonatal Surgery*, 14 (32s), 546-571.

ABSTRACT

Accurate assessment of extraocular muscle dimensions is crucial for diagnosing orbital and systemic pathologies. Computed Tomography (CT) offers high-resolution imaging for precise measurement of orbital structures. This study aims to establish normative values for the diameters of extraocular muscles in a healthy population using CT imaging and to evaluate variations based on age, gender, and laterality. A prospective analysis was conducted on CT head scans of 118 individuals without orbital pathology. Measurements included diameters of the medial, lateral, inferior rectus, and superior muscle groups for both eyes. The study establishes normative CT-based ocular muscle dimensions, providing a reference for clinical assessment in the Indian population.

Keywords: *Ocular Muscle (OM), Computed Tomography (CT), Extraocular Muscles (EOMs), Orbital Measurements (OMeas), Medial Rectus (MR), Lateral Rectus (LR), Inferior Rectus (IR), Ocular Diameter (OD), Lens Density (LD), Right and Left Eye Comparison (RLEC), Age and Gender Variability (AGV)*

1. INTRODUCTION

1.1 INTRODUCTION

CT stands for computed tomography, a diagnostic imaging tool that helps create images of internal structures by integrating X-rays and a computer system. It helps to diagnose various pathologies and can reveal certain body conditions like tumors, internal bleeding, fractures, hemorrhage, and many more. it can show accurate images of bones, fat, muscles, organs, and blood vessels. (1)

1.2 HISTORY

Computed tomography was developed on 1 October 1971. This was an exciting technique used to create carbon copies of the human brain with the help of a computer which is used for processing the data and images are displayed in the monitor. This technology brings a vast change in the field diagnosis of pathology.

The revolutionary machine was first used to scan an adult female patient under the care of Dr. James Ambrose at Atkinson Morley Hospital. The scan revealed a suspected tumor in her frontal lobe, which was later confirmed to be a cystic astrocytoma. Although the imaging process was lengthy and time-consuming, the results proved to be highly valuable. This breakthrough marked the beginning of a new era in diagnostic radiology, offering a non-invasive alternative for identifying various medical conditions. (1)

1.3 Tasks Before Hounsfield

At Cambridge University and Cape Town University, Cormack studied physics. He went back(to South Africa and worked at Groote Schuur Clinic) during the 1950s, regulating the protected treatment of radio nuclide as well as, direct, the utilization of x-beams for conclusion and treatment. He aimed to ascertain this map from transmission measurements through the object, pointing out that the techniques employed for dosimetry were rudimentary compared to those employed in the physical sciences and that accurate x-ray dosimetry could only be achieved with knowledge of the distribution of attenuation

coefficients between the source and the point of interest.He set out to develop a method for measuring the attenuation coefficient of inhomogeneous media because he discovered that while the literature described how to measure the attenuation coefficient of a uniform material, there was no method for measuring it. While his primary inspiration was dosimetry, he perceived that these guides of constriction would have different advantages, remembering disposing of the constraint for radiography because of the way that pictures of district of interest are superimposed on pictures of tissues above and beneath the designs of interest. His progress on this subject was slow because it was a side project that had nothing to do with his main responsibilities at work. In order to tackle for a capacity from its line integrals, Cormack realized that the problem was numerical in nature. After reading the material and speaking with mathematicians in Cape Town, he was unable to find any arrangement and initially came up with a solution for objects that were round even. He had a ghost made out of Aluminum and wood, was able to calculate lessening coefficients for these materials that were very similar to free estimations, and made transmission estimations along equal lines using a Co60 source (only one view was needed because of the round balance). The results were published in 1963. He then extended his idea to objects without circular symmetry. A student named David Hennage supplied the computer processing expertise required for execution. Cormack plotted the attenuation coefficient along the profiles of an aluminum and Lucite phantom he had measured. Perhaps the first experimental demonstration of computer-assisted tomography was made, and the work was good enough to share the Nobel Prize with Hounsfield. The outcomes were distributed in 1964. Years later, in a 1973 publication that included described application to imaging of positron producers and transmission estimations with heavy metal particles, he reviewed papers on recreation by Radon and others. Regarding his 1960s work, Cormack explained, Efforts were made to demonstrate the results to clinic physicists, but to little effect. Around the same time as Hounsfield's work at EMI, but without any information on it, a Siemens team under the direction of Dr. Friedrich Gudden also led work on what was eventually named CT. In 1967, they found that cross-sectional images of attenuation coefficients could be produced using X-ray transmission measurements. Since these researchers were employed in the radiology industry, they may have been reliant on the findings and trends of the discipline at the time. The importance of high spatial goals was one of them. They understood the basic requirements for tomographic remaking and realized that they would need a large number of projections, each with a large number of tests, and they would need to create images with incredibly large framework sizes in order to achieve spatial goals equivalent to radiography.At the time, these computations were beyond the capabilities of PCs. The task was terminated because of these obstacles to achieving the spatial target of a minuscule fraction of a millimeter [and perhaps not fully appreciating the impact of low differentiation perceptibility in three aspects (3D)]. At the same time, Hounsfield and EMI were working on a clinical prototype CT head scanner in the UK, although they were not aware of Cormack or Gudden's earlier work. (1)

1.4 GN Hounsfield and the creation of the first clinical CT system

At the age of 30 Godfrey Newbold Hounsfield became a member of Emi in 1949. in that era Emi was one of the best industries, before joining Emi he used to work in radar at the time of war. He was very fascinated by the basics of technology. After joining Emi, he spent a year working on radar systems and associated displays.Years after joining the industry he directed the first creation of a universal computer transistor in the United Kingdom. His design foundation would demonstrate vital for his benefaction towards medication. At the point when Hounsfield completed his PC work, he moved to EMI's Focal Exploration Lab (CRL), known for advancements in sound system recording and television broadcasting. He wondered if "readings" through a box could reveal what was contained within. He was introduced to medical imaging in 1967 by a doctor, which gave rise to the concept of using light to read a closed book. He used parallel slices to reduce this to a 2D problem. Toward the finish of 1967, he physically determined a 3x3 framework of numbers from various points and, with Stephen Bates, made a program to figure an 8x8 network utilizing fundamental number-crunching. Funding was difficult. He chipped away at the "3D x-beam" thought without financing from November 1967 to July 1968. He applied for a patent by June, but the CRL chief wanted funding from outside sources. The Health and Social Security Department of the United Kingdom (DHSS) declined Hounsfield's request for £10,000 in August. He worked on his proposition and, in October, got £2500 from DHSS and more financing later. A single scan on the first CT scanner, which was constructed from salvaged components, took nine days. This time was cut to nine hours by using an X-ray tube. By 1969, a mainframe computer enabled faster reconstructions. Including James Ambrose, Hounsfield collaborated with radiologists to obtain brain samples. Notwithstanding distrust about CT's lower goal and greater expense contrasted with film, they chose to fabricate a clinical model in the mid-1970s. On October 1, 1971, the primary live persistent CT check showed an astonishing point of interest, outperforming assumptions and changing radiology. Despite initial funding issues and technical difficulties, Hounsfield's persistence paid off. (1)

1.5 BASIC PRINCIPLE

The internal structure can be reconstructed by using multiple projections. Computerized technology and the use of X-rays are used in CT to create precise cross-sectional images of the body. These pictures, called slices, highlight certain anatomical features of the body. The thickness of these slices is selected with collimators to minimize undesired radiation and overlapping pictures. The CT scan data is divided into tiny squares called pixels to produce a grid. Each pixel displays various aspects of the image. Depending on the amount that different materials absorb the x-beam radiation, structures seem darker in the CT images. The straight linear attenuation coefficient, which is dependent on the material's thickness, nuclear number,

and x-beam bar energy, estimates this ingestion. More x-beams are assimilated by denser and more atomic-numbered materials. Tissue identification is facilitated by the measurement of X-ray absorption in Hounsfield units (HU); nevertheless, HU values can occasionally be slightly wrong due to several causes. One problem is shaft solidification, which results in the picture's ancient rarity because low-energy x-beams are kept longer. Aluminum channels can be used to reduce these remnants and improve the quality of images while simultaneously reducing the radiation dose to the patient. Less thick materials appear hazier, whereas denser and nuclear number materials absorbed more x-beams. Certain structures can become a specific therapeutic concern when using contrast agents that include iodine, as they temporarily increase the disparities in density.

Thinner slices are superior at collecting finer features and at reducing volume averaging, which is the blending of normal and aberrant tissues. The strength of the Tissue identification is facilitated by the measurement of X-ray absorption in Hounsfield units (HU); nevertheless, HU values can occasionally be slightly wrong due to several causes. One problem is shaft solidification, which results in the picture's ancient rarity because low-energy x-beams are kept longer. Aluminum channels can be used to reduce these remnants and improve the quality of images while simultaneously reducing the radiation dose to the patient. Less thick materials appear hazier, whereas denser and nuclear number materials absorbed more x-beams. Certain structures can become a specific therapeutic concern when using contrast agents that include iodine, as they temporarily increase the disparities in density.

Thinner slices are superior at collecting finer features and at reducing volume averaging, which is the blending of normal and aberrant tissues. The strength of the Voltage and tube current in a tube in the CT machine's gantry regulate X-ray photons. The machine's identifiers turn the x-beams into electric signals, which are then processed by the DAS (information procurement framework) and processed by the focus handling unit (computer processor) to create images. Usually shown in HU, the pixel values of these images correspond to various physical designs.

Three main phases comprise the operation of CT scanners: information procurement (which involves collecting x-beam data), image reconstruction (which assigns values to each pixel), and picture show (which displays the data in survey-friendly shades of dim). (2)

1.6 CT GENERATIONS

1.6.1 First generation or EMI scanner

EMI's first scanner was created especially for neuroimaging. Between an array of detectors below and an x-ray tube above, the head of this apparatus was submerged in a water bath.

Before the beam reached the patient, a 3rd device—a detector—intercepted a portion of it. x-ray tube was correctly positioned, detected, and its relative position was maintained by a stiff scanner gantry. For the duration of the scan, the patient remained in the same position. Two different types of motion were experienced by the gantry: a rotary kind and a linear kind.(3)

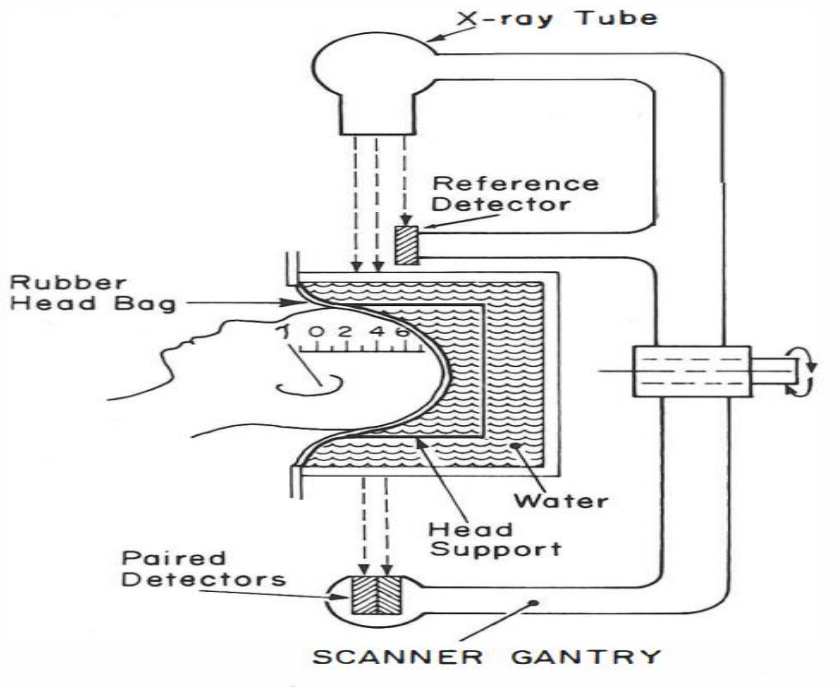

Figure 1.1 The scanner gantry

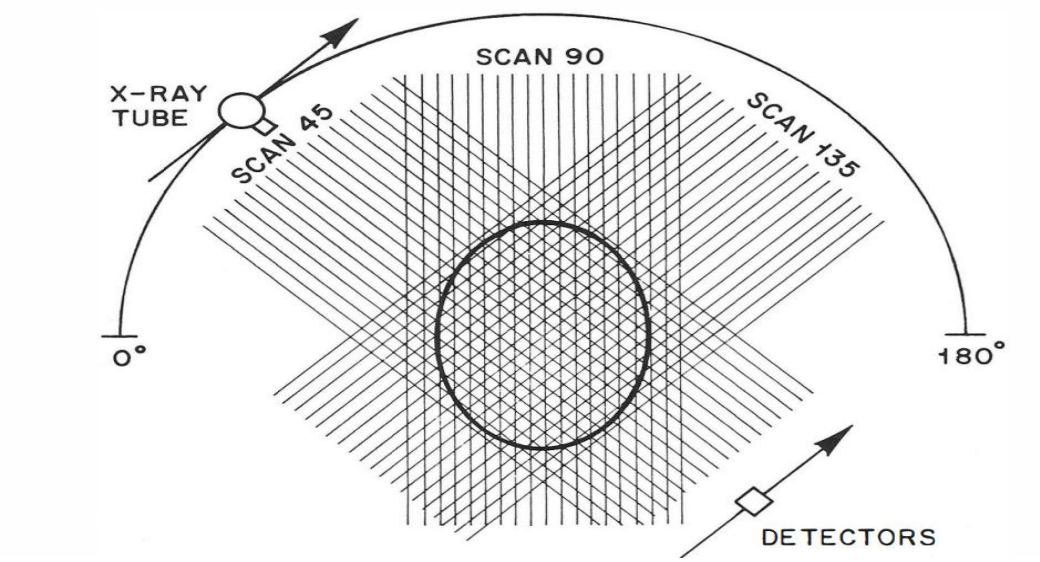

Figure 1.2 First generation or Original EMI Scanner

1.6.2 Motion scanning

Several design modifications have been made to CT scanners since the technology's initial introduction in 1971

It divides into five categories, such as

- **1st generation (translate-rotate, one detector)**
- **2nd generation (translate-rotate, multiple detectors)**
- **3rd generation (Rotate-rotate)**
- **4th generation (Rotate-fixed)**
- **Other geometries**

(a) First generation

Initially EMI device was a scanner from the first generation. It used a single detector for each radiography section, resembling a pencil-shaped x-ray beam. The x-ray tube-detector movements, also known as "translate-rotate motion," were both rotary and linear. A five-view head study required twenty to thirty minutes.(3)

(b) Second generation

A primary goal of second-generation scanners, as well as of all. The aim of subsequent configurations was to reduce the duration of scanning for every tomographic section. The original EMI scanner's pencil beam and single detector were replaced with a (fan-shaped beam and multiple detectors)to achieve the desired speed increase.(3)

(c) Third generation (rotate-rotate)

“The General Electric Company”debuted a scanner in 1975 that completely eliminate translation motion. All that was needed was rotation motion, with the patient being rotated by the x-ray tube and detectors. This scanning geometry became known as- "fan beam" geometry or "third-generation" configuration since(the original equipment could do a scan in 4.9 seconds. (3)

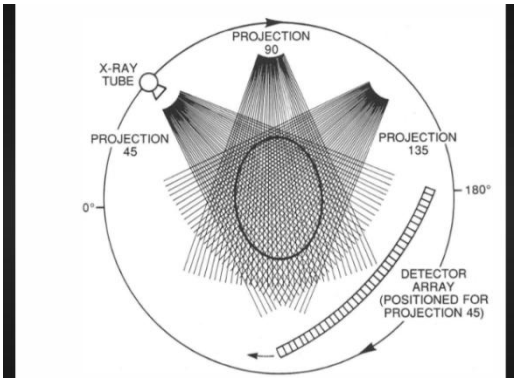

Figure 1.3 rotate- rotate scanner

(d) Fourth generation (rotate -fixed)

The patient is fully surrounded by the ring that the detectors have formed. The detectors remain stationary. The x-ray tube revolves, inside the detector ring, and (the x-ray beam is collimated) to produce a fan beam. The x-ray beam is constantly going through a detector fan. Over 2000 detectors have been used in some designs. The exposed detectors are read, when the xray tube is positioned at specific angle(3)

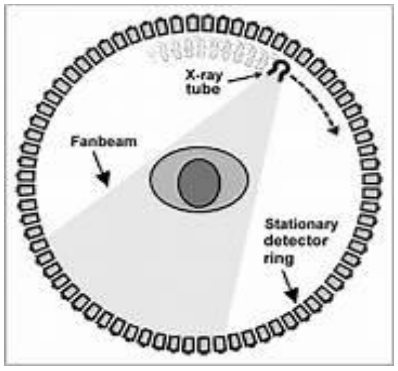

Figure 1.4 rotate-fixed scanner

1.6.3 Other geometries

(a) Electron beam CT

Electronic beams are magnetically focused and deflected to replace the motion of an x-ray tube. This technique is the gold standard technique used in cardiac imaging that puts the patient inside the enormous x-ray tube's radius. A (cardiovascular computed tomography scanner, or CVCT scanner), is term used to describe the instrument.The 3 primary components of the CVCT scanner are a ring of detectors, an electron gun with focusing and deflecting coils, and a 180 cm diameter tungsten target ring.(3)

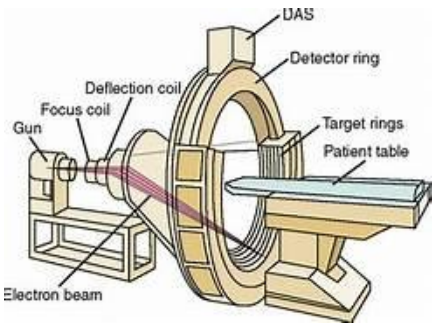

Figure 1.5 electron beam CT

(b) Spiral or helical CT

Helical CT , or spiral CT was introduced in the early 1990s, with much of the development led by (Willi Kalender and Kazuhiro Katada).In helical CT, the x ray source is attached to a freely rotating gantry.During a scan the table moves the patient smoothly through the scanner.It was the development of two technologies that made helical CT Useful: sliding rings to turn on and off the revolving gantry and convey data and power.Additionally, the switched mode power supply is compact enough to mount on the gantry while yet having enough power to supply the x-ray tube.(3)

.

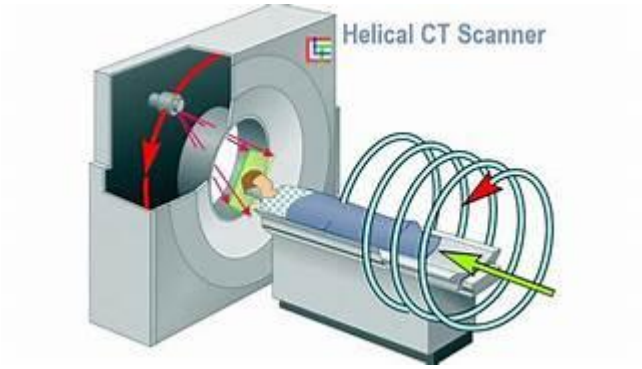

Figure 1.6 spiral or helical CT scanner

(c) Multi slice CT scanner

The idea behind multi-slice CT scanners is similar to that of helical or spiral CT scanners, except they have many detector rings.The resolution is higher than that of single-slice scanners used in high-resolution CT procedures. The faster volume coverage is the main advantage of multi-slice CT. This makes it possible to scan big volumes at the best moment.(3)

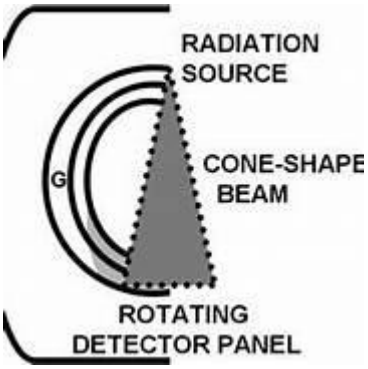

Figure 1.7 multi-detector CT

Figure 1.8 multi detector CT scanner

1.7 CT Instrumentation

(a) X ray tube

For CT to work optimally, the radiation source should provide a monochromatic Xray beam one composed of photons with the same wavelength. It is simpler and more precise to rebuild an image using a monochromatic beam. Earlier generations used rather large (2 X 16 mm) fixed-anode, oil-cooled focal spot tubes operating at around 30 mA and 120 kV (constant potential). To raise the radiation's mean energy and exclude low-energy photons, the beam underwent extensive filtering.(3)

The new fan beam units feature a diagnostic X-ray tube with a rotating anode and a significantly smaller focal spot (0.6 mm in certain models. These tubes can tolerate the extremely high heat loads produced when several slices are acquired quickly one after the other because to their large heat loading and heat dissipation capacities. There are anode heat capacities of up to 3,500,000 heat units and the ability to have tube currents exceeding 600 mA.(3)

(b) Collimators

a) The X-ray beam is collimated in two separate areas: close to the X-ray tube and at the detector. It is imperative that the two are perfectly aligned. The only tool available for managing scatter radiation is the collimator located at the detector. Every detector possesses a unique collimator. Additionally, the collimators control the tomographic slice's thickness, or voxel length.Most scanners feature adjustable collimators that allow for varying slice thicknesses, typically ranging from 1 to 10 or 15 mm.(3)

(c) Detectors

b) CT scanners primarily use two types of detectors: scintillation crystals and xenon gas ionization chambers.

The only rotate-rotate (or "third-generation") type scanners that can use xenon gas ionization detectors are those that also include scintillation crystal detectors. The "fourth generation" of rotate-fixed scanners requires the use of scintillation crystal detectors.(3)

(d) Image reconstruction-

c) In computed tomography, a cross-sectional slice of the body is segmented into numerous small blocks.

Every block is given a number that corresponds to how much,the block attenuated the x-ray beam. The individual blocks are called the voxels.

To quantify attenuation, one uses the linear attenuation coefficient (μ).(3)

1.8 Algorithms for Image Reconstruction

Creating an accurate cross-sectional presentation of each element in the image matrix's linear attenuation coefficients is the goal of all the methods.(3)

(a) Back -projection-

Often referred to as the "summation method," back-projection is the most ancient technique for reconstructing images. Not one of the CT scanners sold in stores use basic back-projection, but since it is the simplest to understand.(3)

1.9 CT Number and Hounsfield unit

d) The digital value of each pixel is called Hounsfield unit. The CT scanner calculates the linear attenuation coefficient for each pixel using the data it gathers.(3)

The “linear attenuation coefficient” of each pixel is determined by the CT computer, and the result is translated to a new integer known as a "CT" number.(3)

e) The connection between a pixel's linear attenuation coefficient and the attenuation coefficient of water, μ, is expressed through the following equation:

$$\text{Ct number} = K\frac{(\mu pixel - \mu water)}{\mu water}$$

* **k= magnification constant**
* **μp= pixel linear attenuation coefficient**
* **μw= water linear attenuation coefficient**

f) In contemporary CT systems, the constant K is set to 1000. With this K value, the CT number for air is -1000, water remains at 0, and dense bone is assigned a CT number of 1000. (3)

g)

1.10 CT POST-PROCESSING TECHNIQUES

h) **Multiplanar reformation or MPR**

MPR can recreate coronal, sagittal, and other (oblique) slice planes from the original 3D volume data in addition to transverse slices.The axial (transverse) plane is the standard orientation for viewing CT images, as it facilitates symmetry analysis and captures closely positioned anatomical structures, such as the liver, pancreas, gallbladder, and bile ducts, which often appear together in a single image. Nonetheless, alternative imaging planes may be more appropriate for specific evaluations. For instance, the sagittal plane is optimal for visualizing midline and longitudinal structures, including the spine, pituitary gland, and uterus.The optimum coronal plane it is crucial for observing longitudinally oriented structures like the lungs, some brain gyri, and long bones when assessing symmetry. To save money on data storage, some hospitals choose not to use MPR on all CT scans. However, MPR permits enhanced musculoskeletal system visualization for evaluating fracture patterns and the tendons, ligaments, and cartilage stabilizing obliquely-coursed joints. Enhancing the display of curved structures, such as the appendix, and improving the assessment of whether potential discoveries are legitimate discoveries or photo artifacts.(3)

i) **Volume rendering technique (VRT)**An algorithm is used by the volume rendering technique (VRT) to give a voxel a final value.

j) **3DVR stands for 3D Volume Rendering** - 3DVR aims to create a fully 3D appearance for constructions. This method works well for evaluation. Structure sizes, including artery hypoplasia and aneurysm size intricate patterns, the connection between two tissues, like when a neighboring artery is encircled by a metastatic bone tumor.(3)

k) **Shaded Surface Display (SSD)**— Depending on a preset range of human eyes, surface rendering, or SSD, determines which voxels to display. SSD inserts or removes voxels from the image using techniques that are intended to detect density differences near the edge, of structure's where surfaces are of different densities. (2)

l) **MIP (Maximum Intensity Projection) -** Voxels with the highest density (HU) are shown by MIP on each view through the volume of the 3D picture. Compared to SSD, MIPs provide a clearer image of high-density structures like bone and arteries loaded with contrast. MIP are widely utilized in CT arteriography, including pulmonary artery emboli detection.

m) **Minimal Intensity Projection** —refer to the following figure— The lowest density voxels are displayed by MinIP. MinIP works well for highlighting structures with lots of air, like the bronchial tree. (4)

1.11 ANATOMY

❖ **EXTRAOCULAR MUSCLE**

n) The seven muscles that are situated inside each circle and are connected to the eyeball are called the extraocular muscles, or superfluous muscles of the eyeball. The four rectus muscles include the medial, lateral, superior, and inferior rectus. The two oblique muscles are the superior and inferior obliques. The levator palpebrae superioris is the sole muscle responsible for elevating the eyelids.(5)

❖ **INVOLUNTARY MUSCLE**

o) The superior tarsal muscle, situated deeper than the levator palpebrae superioris, attaches to the upper edge of the superior tarsus and functions to elevate the upper eyelid. The fascial sheath of the inferior rectus and inferior oblique links to the inferior tarsal muscle, positioned at the lower edge of the inferior tarsus, which may cause the lower eyelid to lower. The orbitalis muscle, located over the inferior orbital fissure, exhibits inconsistent behavior.(5)

❖ **VOLUNTARY MUSCLE**

There are four recti muscle

- SR (Superior rectus)
- IR (Inferior rectus)
- MR (Medial rectus)
- LR (Lateral rectus)
- Two oblique muscles
- SO (superior oblique)
- IO (Inferior oblique)

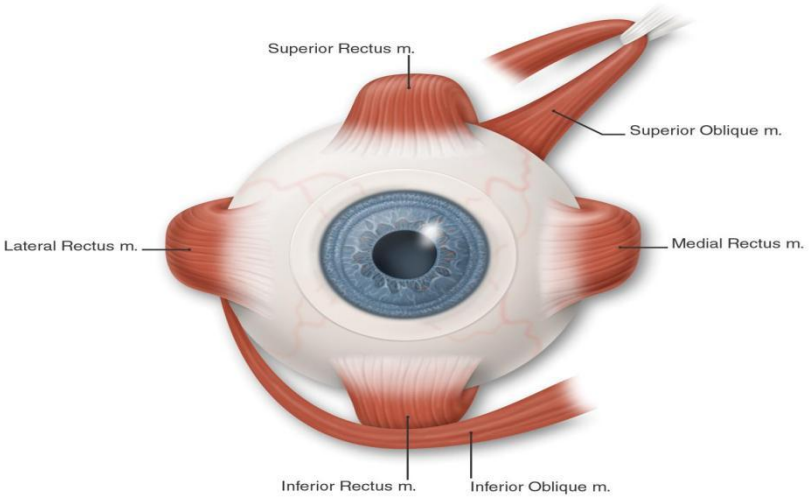

Fig1.9 - represents extraocular muscle

❖ **ORIGIN OF OCULAR MUSCLE**

p) The lateral rectus features a small tendinous head arising from the orbital surface of the sphenoid bone's greater wing, positioned laterally to the tendinous ring. The abducent nerve passes between these two heads. The superior oblique originates from the undersurface of the sphenoid's lesser wing, located superomedially to the optic canal. The inferior oblique starts on the maxilla's orbital surface, lateral to the lacrimal groove, and is positioned along the anterior edge of the orbit.(5)

q) The levator palpebrae superioris arises from the orbital surface of the sphenoid bone's lesser wing, positioned anterior to the optic canal and the origin of the superior rectus.(5)

❖ **STRUCTURE AND FUNCTION**

r) The eyes are in primary gaze when the head is upright and the eyes are directed directly ahead. An extraocular muscle activation from this place results in a secondary or tertiary action. Although the eye can rotate approximately 50 degrees from its primary position during normal movements, only about 15 degrees of extraocular muscle motion occur before head movement begins. The rectus and oblique muscles manage the eye's different gaze directions.(5)

The closest point at which the muscle initially makes contact with the globe is the functional insertion point of each rectus and oblique muscle. This point creates the "arc of contact," a tangential line, that runs from (the globe to the beginning of the muscle). The rectus muscles are located at the orbital apex of the "Annulus of Zinn," which explains , same point of origin. Instead of touching the globe directly, the levator palpebrae superioris lifts the eyelid.(5)

❖ **BLOOD FLOW AND LYMPHPATIC SYSTEM**

s) The primary blood supply to the extraocular muscles is provided by the lacrimal artery, infraorbital artery, and muscular branches of the ophthalmic artery.

t) The ocular artery divides into two branches: the superior and inferior muscular branches. The lateral rectus is supplied by a branch of the lacrimal artery, while the other rectus muscles receive blood from two anterior ciliary arteries connected to the anterior ciliary body circle. Similar to the arterial system, venous drainage flows into the superior and inferior orbital veins.(5)

The vortex veins are typically positioned adjacent to the superior and inferior rectus muscles, both on the medial and lateral aspects. They connect to and drain into the orbital venous system.(5)

❖ **NERVE**

The lower branch of the third cranial nerve (oculomotor nerve) supplies the inferior rectus, medial rectus, and inferior oblique muscles. Its upper branch innervates the superior rectus and the levator palpebrae superioris. The fourth cranial nerve (trochlear nerve) controls the superior oblique muscle, while the sixth cranial nerve (abducens nerve) is responsible for innervating the lateral rectus muscle. (5)

❖ **MUSCLE**

Each rectus muscle originates, posteriorly at the "Annulus of Zinn" and proceeds anteriorly along the orbital walls to the place of insertion.

The insertion positions of these muscles vary in distance from the limbus on the globe, and the curving line that forms a spiral along these insertion points is called the Tillaux spiral. Starting at the medial aspect of (the globe, the medial rectus, inferior rectus, lateral rectus, and superior rectus all insert at varying distances from the limbus,).The superior oblique begins medial, to the optic foramen and passes through the orbital rim's superonasal region through the trochlea, a pulley. From here, the muscle passes beneath the SR and attaches itself somewhat below the latter's point of entry. The LPS (levator palpebrae superioris) runs anteriorly and arises from the sphenoid's lesser wing. The muscle's body passes across the superior rectus and moves in the direction of the eyelid. The LPS (levator palpebrae superioris) fibres undergo a shift in direction at this ligament, becoming more vertical, and they split to form the superior tarsal muscle superiorly and the aponeurosis anteriorly. EOM include a sizable ratio of nerve fibers, to skeletal muscle fibers. It is 1:3 to 1:5 in relation to other skeletal muscles, which range from 1:50 to 1:125. The skeletal muscle form known as extraocular muscles is specialized and has several types of muscle fibres, such as saccadic (rapid) muscle fibres and slow tonic forms that withstand exhaustion.(5)

❖ **VARIENT IN PHYSIOLOGY**

The extraocular muscles differ in size, attachment sites on the eyeball in relation to the limbus, and various structural traits from one individual to another. These anatomical variations are normal, and no two people have identical muscle configurations or insertion points on the globe.

Auxiliary extraocular muscles that arise from the Annulus of Zinn and are positioned in various locations have been reported on occasion. Both supernumerary muscles and auxiliary extraocular muscles have been described.

Ocular misalignment, may be brought on by congenital variations in the EOM'S.(5)

2. AIM AND OBJECTIVE

2.1 Aim

To provide baseline measurement for the thickness in extraocular muscle in up west population

To assist clinicians accurately assesting extraocular muscle condition

2.2 Objective

- To measure the diameter of ocular muscle
- To establish normative data for the thickness of extraocular muscle.
- Data is essential for understanding normal muscle dimension in up west population

3. NEED OF THE STUDY

- This study has not been performed in the UP-West population
- Accurately determining the ocular muscle's dimensions, location, and diameter aids radiologists, ophthalmologists, and surgeons in diagnosing pathology.
- Is useful for tracking Graves' illness, where inflammation can cause muscles to enlarge

4. MATERIAL METHODLOGY

4.1 STUDY SITE

Data collected from Teerthanker Mahaveer Hospital and Research Center, Moradabad, by using computed tomography (Philips ingenuity 128 slice).

4.2 TYPE OF STUDY-

This prospective study was conducted in the Department of Radio-Diagnosis at Teerthanker Mahaveer Hospital and Research Centre, located in Moradabad.

4.3 DESIGN OF STUDY

It is a CSS (cross-sectional study) that helps to check the dimensions of ocular muscle

4.4 STUDY DURATION

This study was done for 1 year at Teerthanker Mahaveer Hospital and Research Center Moradabad

4.5 STUDY POPULATION

Western Uttar Pradesh

4.6 PARTICIPANTS

Data of the patients coming for NCCT head is acquired from the department of radio-diagnosis, both OPD and IPD patients were included in the study.

4.7 SAMPLE SIZE

118 patients

4.8 SAMPLING METHOD

Convenient sampling

4.9 INCLUSION CRITERIA

- Patients aged ranging from 10 to 62 years were included
- CT head patients were included
- Nontraumatic patient

4.10 EXCLUSION CRITERIA

- All patients with soft tissue injuries in or around the eyes, facial disorders, or fractures of the maxillary, orbital, or skull were not included.
- Individuals who underwent intraocular lens surgery to treat cataracts were not included.
- Individuals with motion artifacts are not accepted.

4.11 ARMAMENTARIUM

Figure 4.1 – United imaging 160 slice CT machine

4.12 MATERIAL AND METHOD

118 sample age ranging between 10 - 62 year old and the sample where collected from the (department of radiology Teerthanker Mahaveer hospital And research Centre Moradabad, Uttar Pradesh)

In this study we measure Normative measurements of ocular muscle using computed tomography. Computed tomography united imaging 160 slice machine was used. Data was collected from the hospital and was measured from Radian Di-com viewer. And performed a statistical analysis on all those collected evaluates of ocular muscle and lens density. Which was taken by me during research projects

These are parameters-

- (Ocular muscles)
- MR (Medial rectus)
- LR (Lateral rectus)
- SR (Superior rectus)

- IR (Inferior rectus)
- LD (Lens density)

Statistical analysis:

The descriptive statistics of F (frequency, % (percentage), average (mean), and SD (standard deviation) were used to summarize the data that was gathered. Age, ocular muscle diameter, and lens density were compared between males and females using the independent sample "t" test. The diameter of the ocular muscle and the density of the lenses were compared between the right and left sides using the Paired "t" test.The Pearson correlation coefficient ("r") was utilized to determine the relationship between age, lens density, and the different ocular muscle diameters. Gender was determined based on lens density and ocular muscle diameter using the Binary logistic regression model. A p-value of < 0.05 was deemed significant. Version 29.0.10 of the SPSS software (SPSS Inc.; Chicago, IL) was used to review data.

5. RESULT

118 patients participated in our prospective cross-sectional study, of whom 78 were male and 40 were female. They were referred to the 'Department of Radio-Diagnosis' at "Teerthanker Mahaveer Hospital," which is run by the 'College of Paramedical Sciences' at "Teerthanker Mahaveer University Research Center, Moradabad

Table 5.1: Descriptive Statistics for age

(n = 118)	Range	Mean	S.D.
Age (Years)	10 to 62	39.00	15.45

Age (of the participants ranged from) - 10 to 62 years with mean: 39.00 $\pm$ 15.45. [Table – 1]

Table 5.2: Gender distribution

		Frequency	%
Gender	M	78	66.1
	F	40	33.9

Among the 118 participants; the majority were males (66.1%); and the 33.9% were females. [Table – 2]

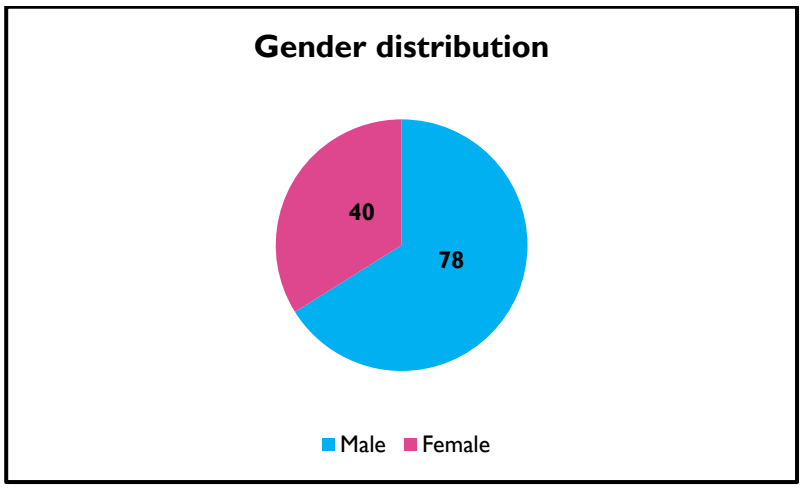

Graph 5.1 represents the gender distribution

Table 5.3: Comparing age according to gender

		Mean	S.D.	"t"	p value
Age (Years)	Male	38.53	15.69	-0.46	0.643
	Female	39.92	15.14		

("t" = Independent sample "t" test)

The Independent sample "t" test was used to compare age; according to gender. There was no difference ($p > 0.05$) in the age between males and females. [Table – 3]

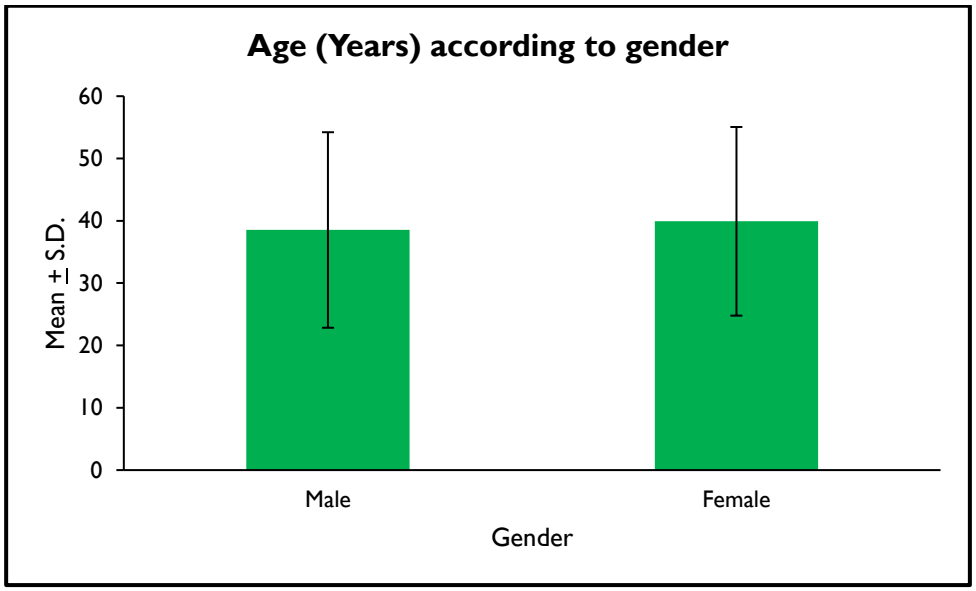

Graph 5.2 represents age(years) according to gender

Table 5.4: Diameter of ocular muscle, and lens density between right and left sides

		Mean	S.D.	"t"	p value
Medical rectus	Right	4.50	0.63	-0.29	0.770
	Left	4.52	0.68		
Lateral rectus	Right	4.02	0.74	-1.56	0.122
	Left	4.11	0.78		
Inferior rectus	Right	4.68	1.00	4.46	< 0.001*
	Left	4.34	0.77		
Superior rectus	Right	4.43	1.03	0.87	0.384
	Left	4.36	0.98		
Lens density	Right	77.89	13.42	0.34	0.738
	Left	77.29	11.85		

("t" = Paired "t" test; * Significant)

The Paired "t" test was used to compare diameter of ocular muscle as well as lens density; between right and left sides. There was a difference ($p < 0.05$) in inferior rectus; between right and left sides. [Table – 4]

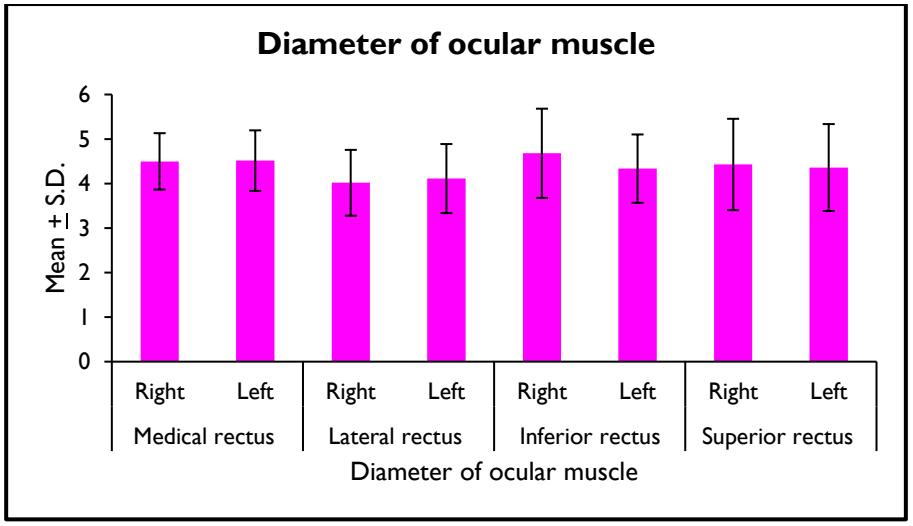

Graph 5.3 represents diameter of ocular muscle

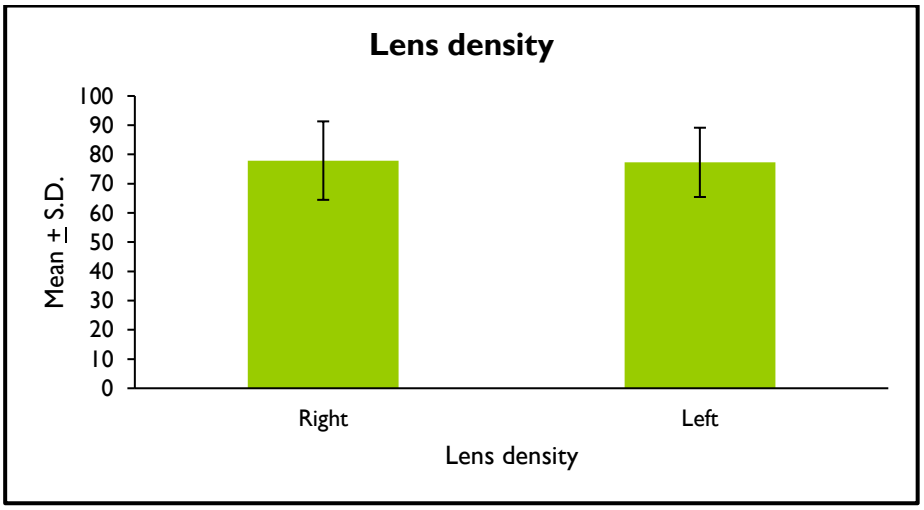

Graph 5.4 represents lense density

Table 5.5: Normative range for diameter of ocular muscle, and lens density

		Normative range
Medical rectus	Right	3.23 to 5.77
	Left	3.16 to 5.88
Lateral rectus	Right	2.54 to 5.49
	Left	2.56 to 5.66
Inferior rectus	Right	2.67 to 6.68
	Left	2.80 to 5.87
Superior rectus	Right	2.38 to 6.48
	Left	2.41 to 6.31
Lens density	Right	51.05 to 104.73
	Left	53.58 to 101.00

Table 5.6: Comparison of diameter of ocular muscle, and lens density according to gender

		Male		Female		"t"	p value
		Mean	S.D.	Mean	S.D.		
Medical rectus	Right	4.52	0.65	4.45	0.61	0.55	0.585
	Left	4.50	0.71	4.55	0.63	-0.37	0.711
Lateral rectus	Right	4.11	0.73	3.83	0.73	1.98	0.050*
	Left	4.24	0.75	3.87	0.77	2.52	0.013*
Inferior rectus	Right	4.79	1.00	4.45	0.98	1.76	0.081
	Left	4.37	0.78	4.26	0.75	0.75	0.455
Superior rectus	Right	4.53	1.08	4.23	0.90	1.55	0.124
	Left	4.38	0.98	4.32	0.98	0.31	0.756
Lens density	Right	77.81	13.83	78.05	12.75	-0.09	0.927
	Left	76.22	11.91	79.38	11.60	-1.38	0.172

("t" = Independent sample "t" test; * Significant)

The Independent sample "t" test was used to compare diameter of ocular muscle as well as lens density; according to gender. There was a difference ($p < 0.05$) in the lateral rectus (Both right and left); between males and females. [Table – 6]

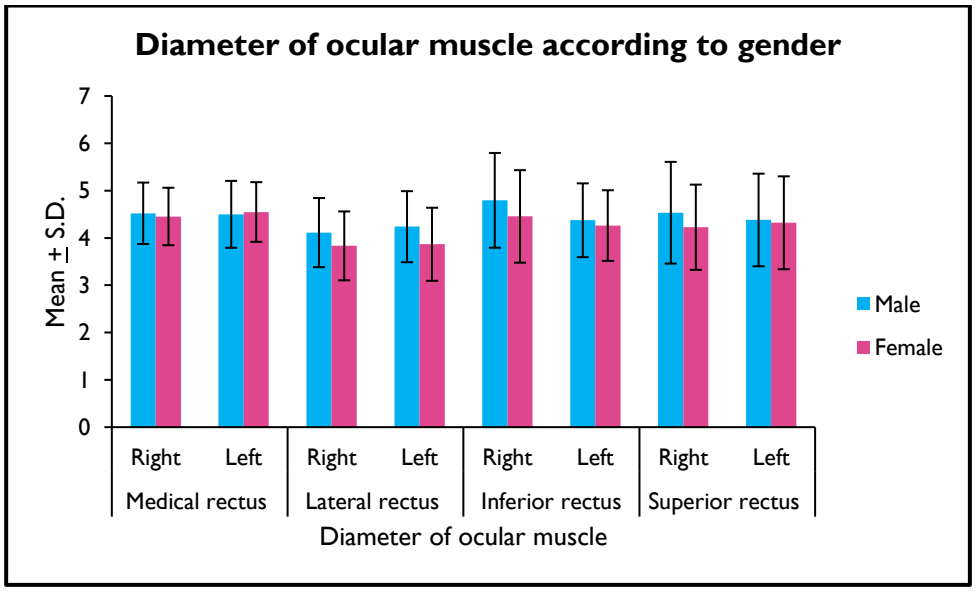

Graph 5.5 represents Diameter of ocular muscle according to gender

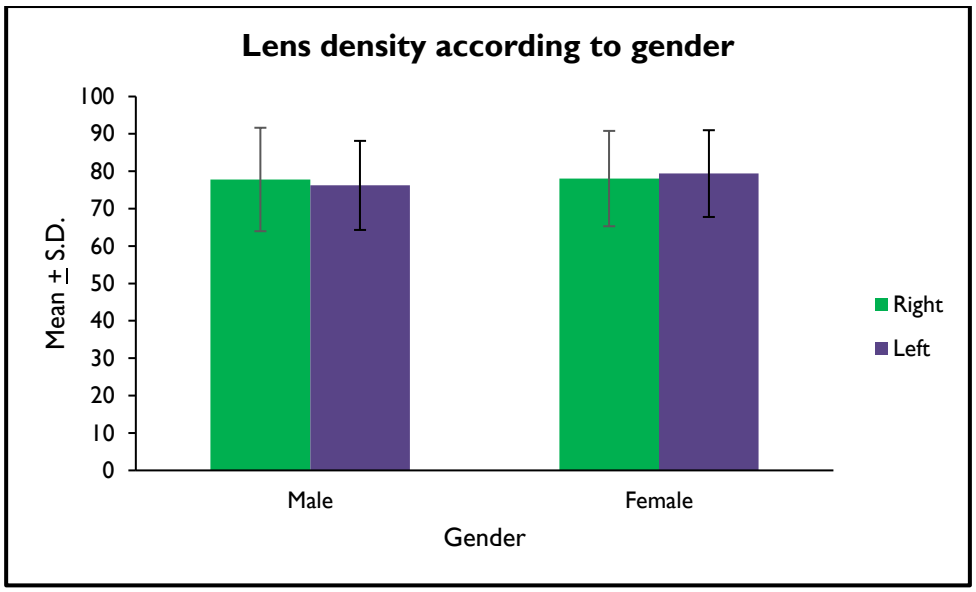

Graph 5.6 represents lens density according to gender

Table 5.7: Relation between the various diameter of ocular muscles, and lens density

			Medical rectus	Lateral rectus	Inferior rectus	Superior rectus	Lens density
Right	Medical rectus	"r"	1	0.460	0.453	0.286	0.170
		p value	--	< 0.001*	< 0.001*	0.002*	0.066
	Lateral rectus	"r"		1	0.379	0.417	-0.136
		p value		--	< 0.001*	< 0.001*	0.143
	Inferior rectus	"r"			1	0.356	0.021
		p value			--	< 0.001*	0.822
	Superior rectus	"r"				1	-0.067
		p value				--	0.472
	Lens density	"r"					1
		p value					--
Left	Medical rectus	"r"	1	0.486	0.483	0.374	-0.091
		p value	--	< 0.001*	< 0.001*	< 0.001*	0.328
	Lateral rectus	"r"		1	0.427	0.455	-0.239
		p value		--	< 0.001*	< 0.001*	0.009*
	Inferior rectus	"r"			1	0.558	-0.089
		p value			--	< 0.001*	0.337
	Superior rectus	"r"				1	-0.057
		p value				--	0.541
	Lens density	"r"					1
		p value					--

("r" = Pearson correlation coefficient; * Significant)

The Pearson correlation coefficient: ("r") was used to find the relation between the various diameter of ocular muscles; and lens density. The medical rectus was positively correlated ($p < 0.05$) with lateral rectus, inferior rectus, and superior rectus; among right as well as left sides. The lateral rectus was positively correlated ($p < 0.05$) with inferior rectus and superior rectus; among right as well as left sides. The Inferior rectus was positively correlated ($p < 0.05$) with Superior rectus; among right as well as left sides. Also, there was a negative correlation ($p < 0.05$) between lateral rectus and lens density; among the left side. [Table – 7]

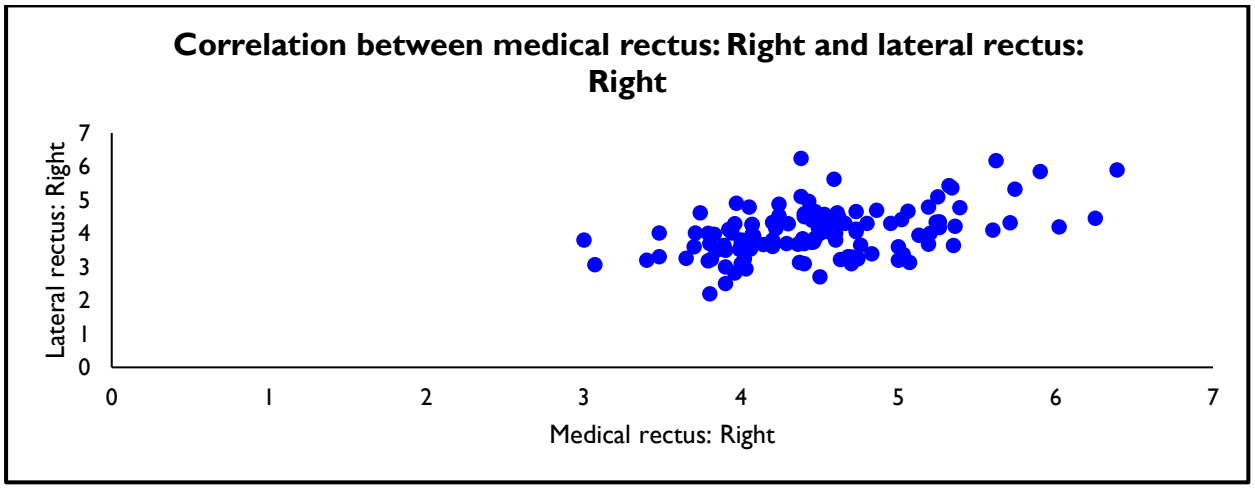

Graph 5.7 represents Correlation between medial rectus: Right and lateral rectus right

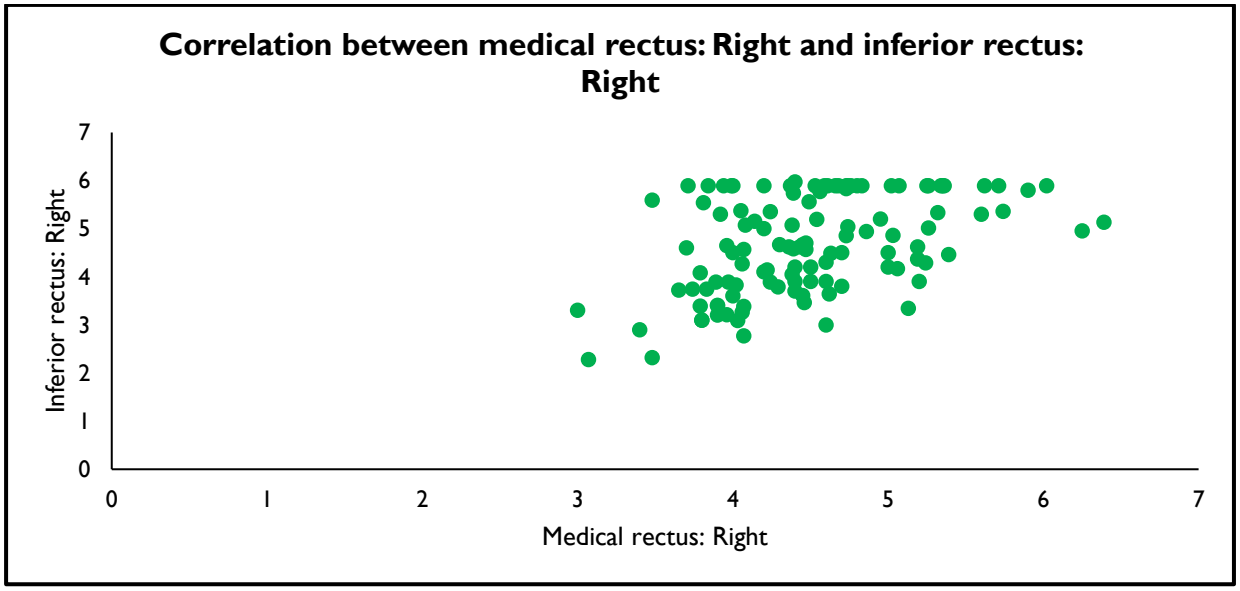

Graph 5.8 represents Correlation between medial rectus:Right and inferior rectus: right

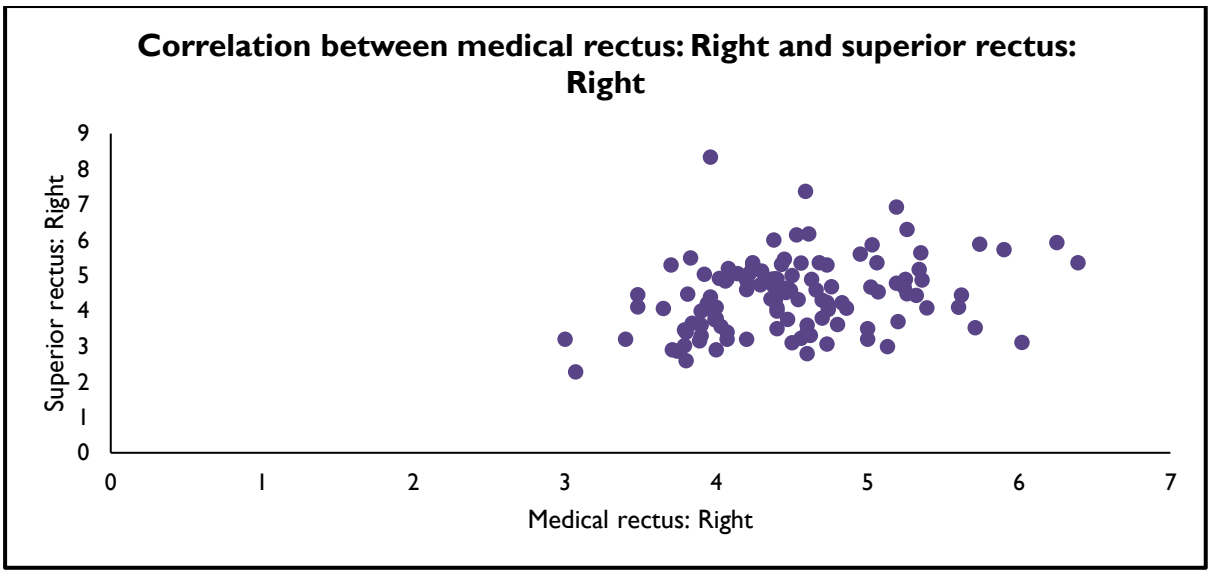

Graph 5.9 represents correlation between medial rectus:Right and superior rectus:Right

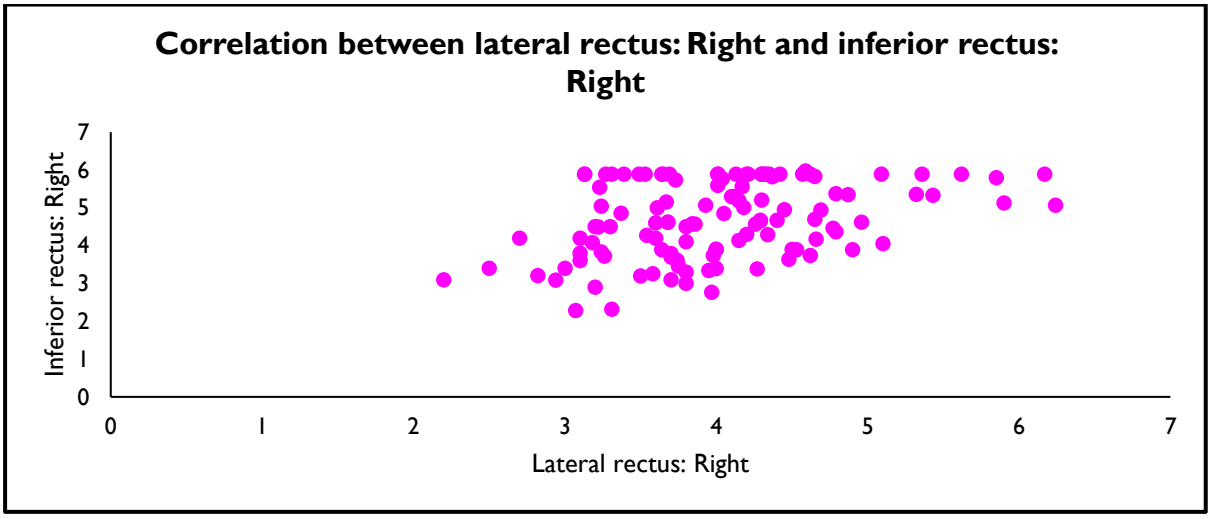

Graph 5.10 represents Correlation between lateral rectus: right and inferior rectus: right

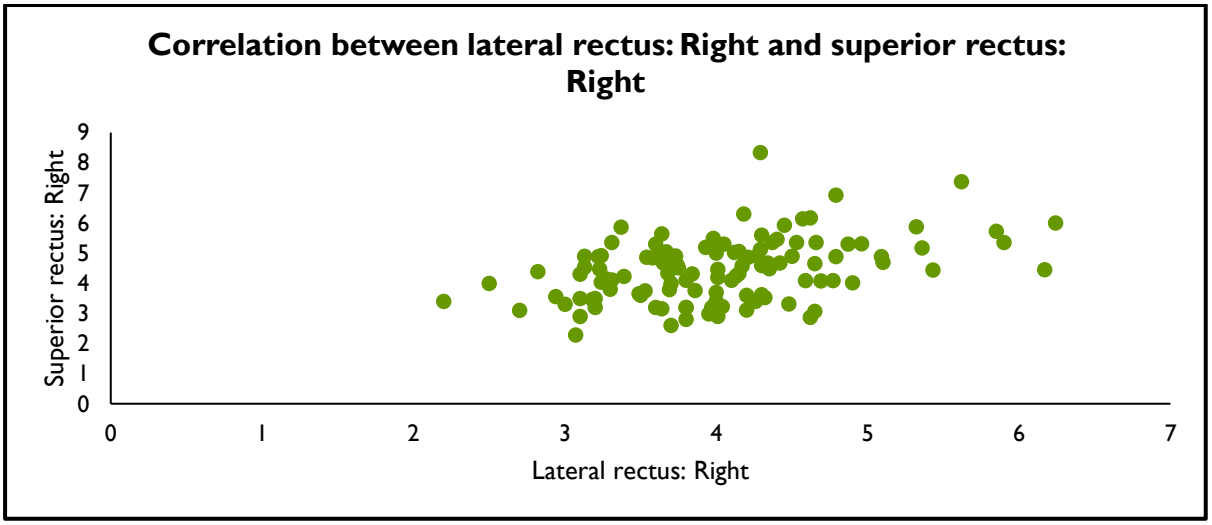

Graph 5.11 represents Correlation between lateral rectus: Right and superior rectus: Right

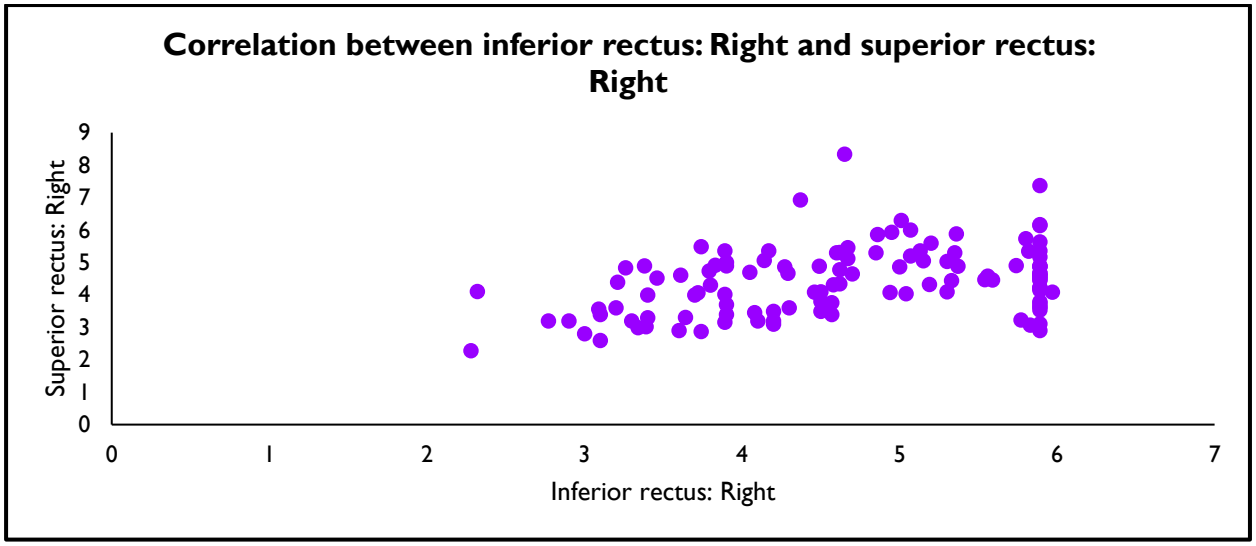

Graph 5.12 represents Correlation between inferior rectus:Right and superior rectus:right

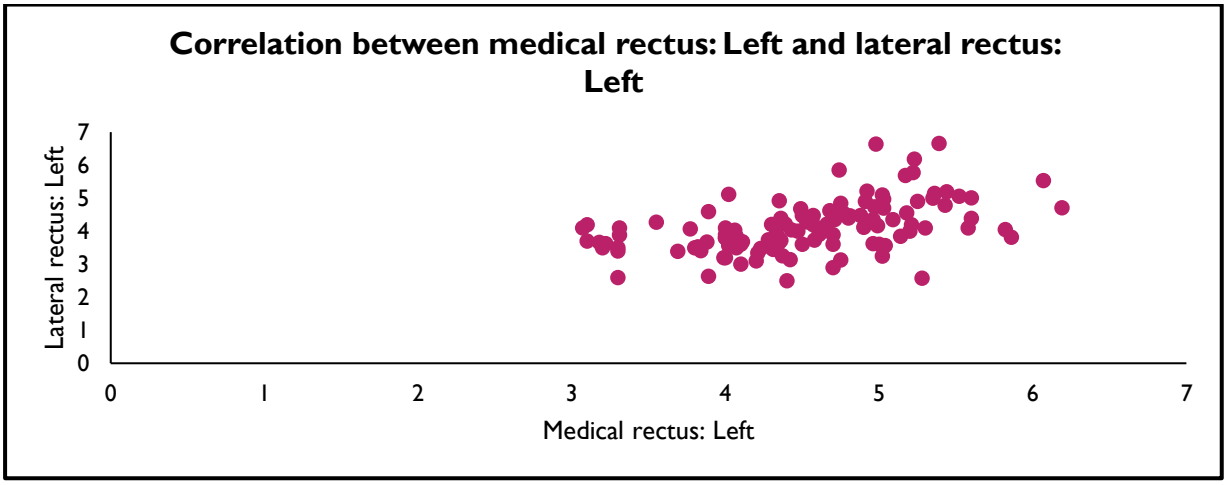

Graph 5.13 represents Correlation between medial rectus: left and lateral rectus: left

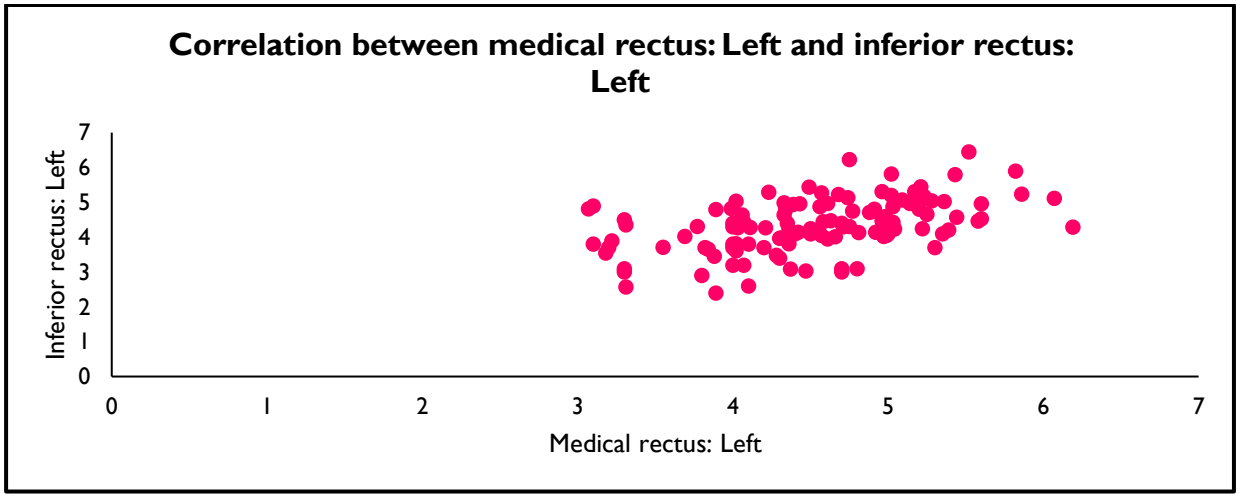

Graph 5.14 represents correlation between medial rectus:Left and inferior rectus:Left

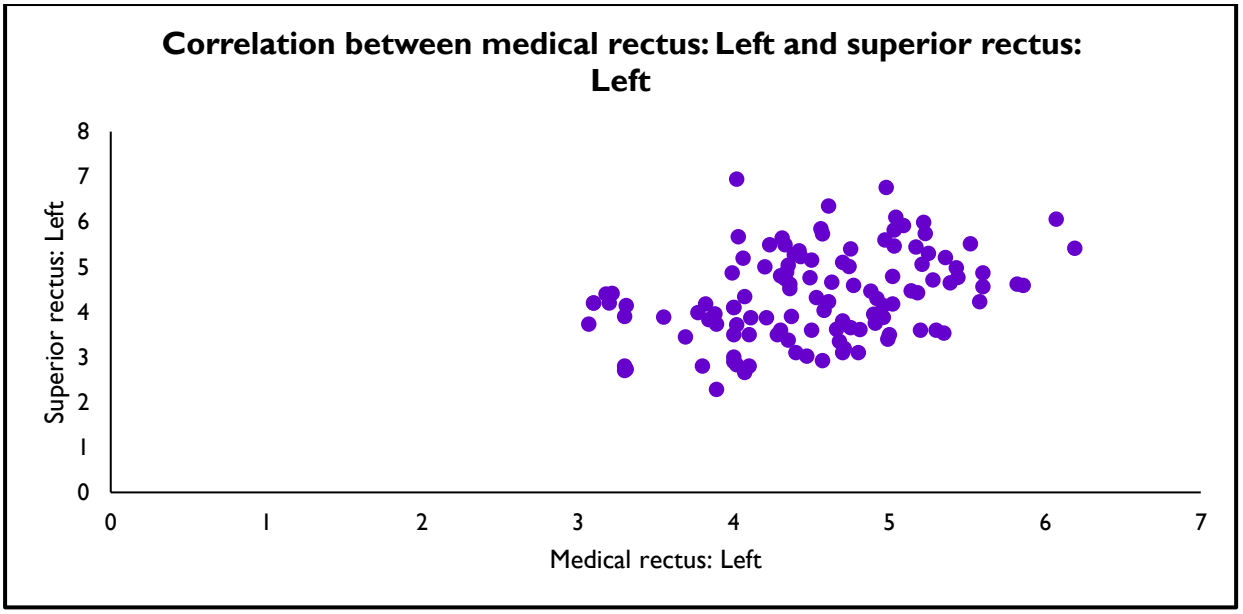

Graph 5.15 represents Correlation between medial rectus:Left and superior rectus:Left

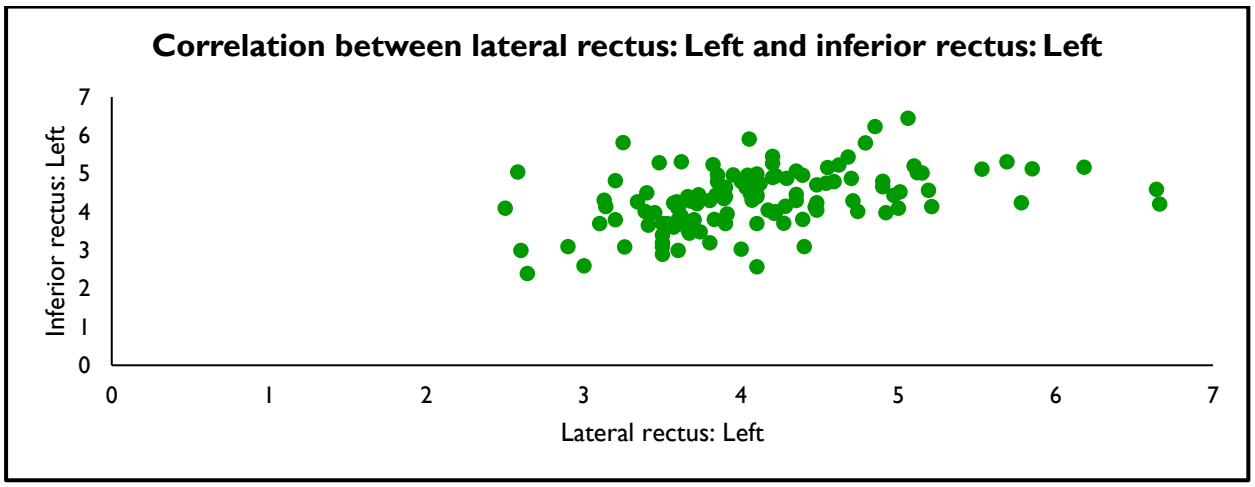

Graph 5.16 represents Correlation between lateral rectus:Left and inferior rectus:Left

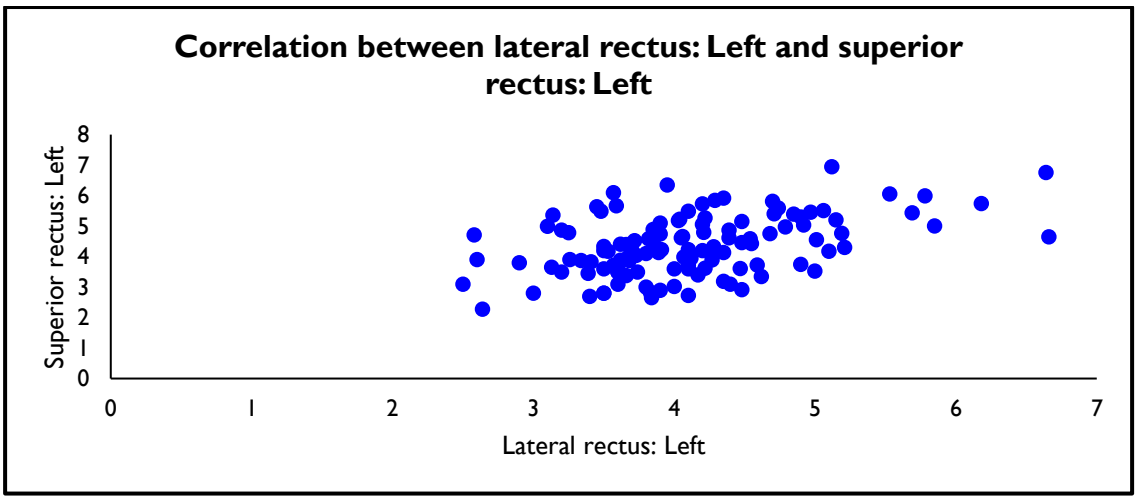

Graph 5.17 represents Correlation between lateral rectus:Left and superior rectus:Left

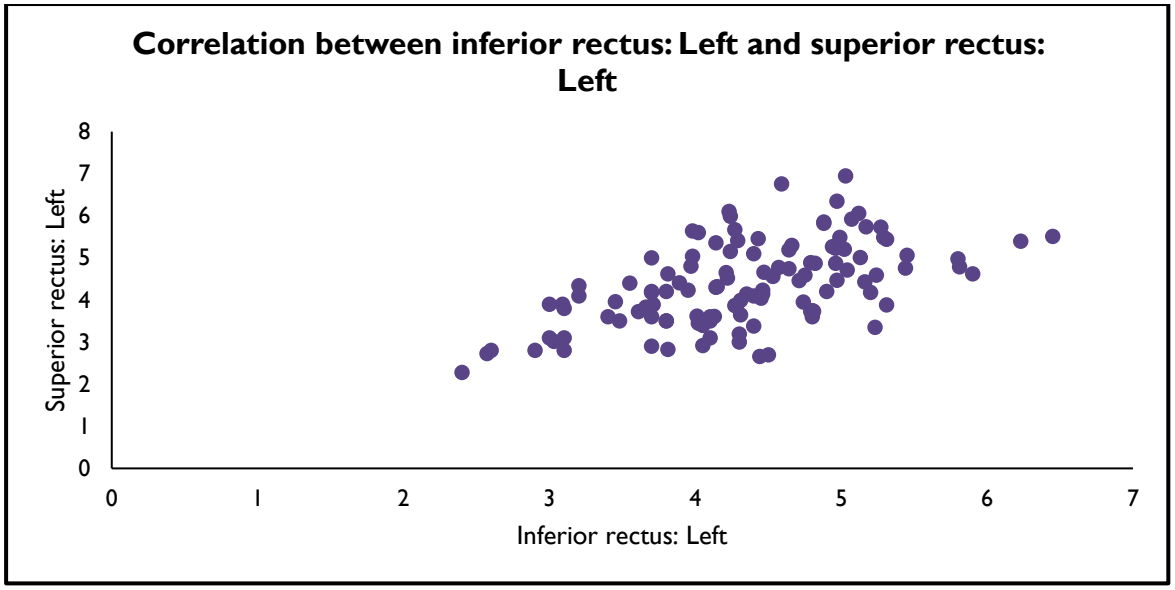

Graph 5.18 represents Correlation between inferior rectus: Left and superior rectus: Left

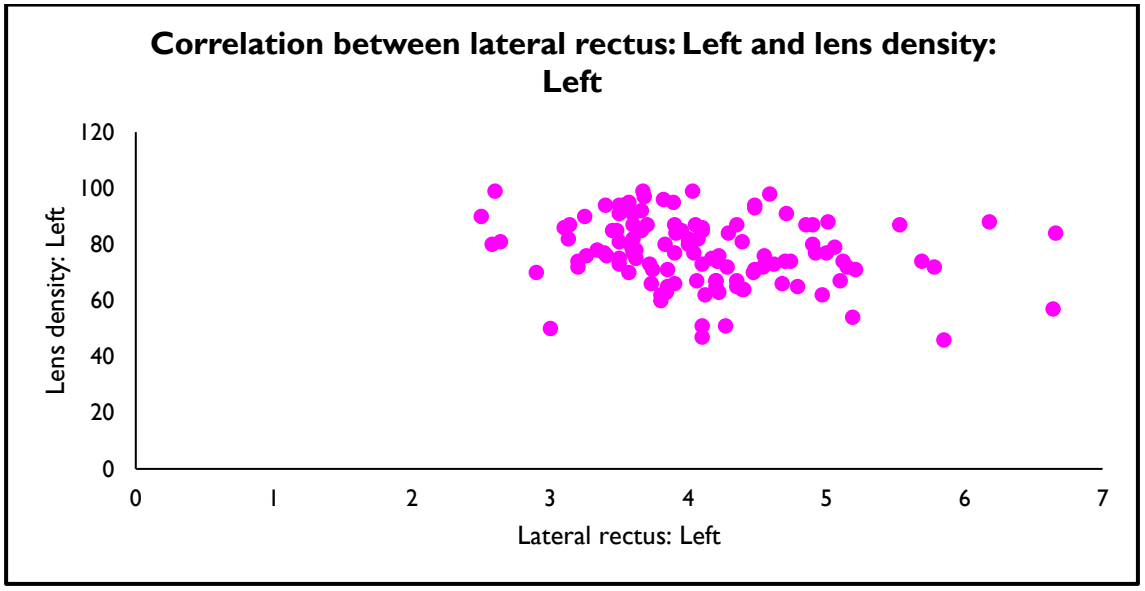

Graph 5.19 represents Correlation between Lateral rectus: Left and Lens density: left

Table 5.8: Relation of the various diameter of ocular muscles, and lens density with age (Years)

		Age (Years)	
		"r"	p value
Medical rectus	Right	0.122	0.188
	Left	0.047	0.614
Lateral rectus	Right	0.177	0.055
	Left	0.175	0.058
Inferior rectus	Right	0.012	0.897
	Left	0.030	0.743

Superior rectus	Right	0.154	0.096
	Left	0.202	0.028*
Lens density	Right	-0.087	0.347
	Left	0.129	0.165

("r" = Pearson correlation coefficient; * Significant)

The Pearson correlation coefficient: ("r") was used to find the relation of diameter of ocular muscles, and lens density with age. There was a positive correlation ($p < 0.05$) between superior rectus (Left) and age (Years). [Table – 8]

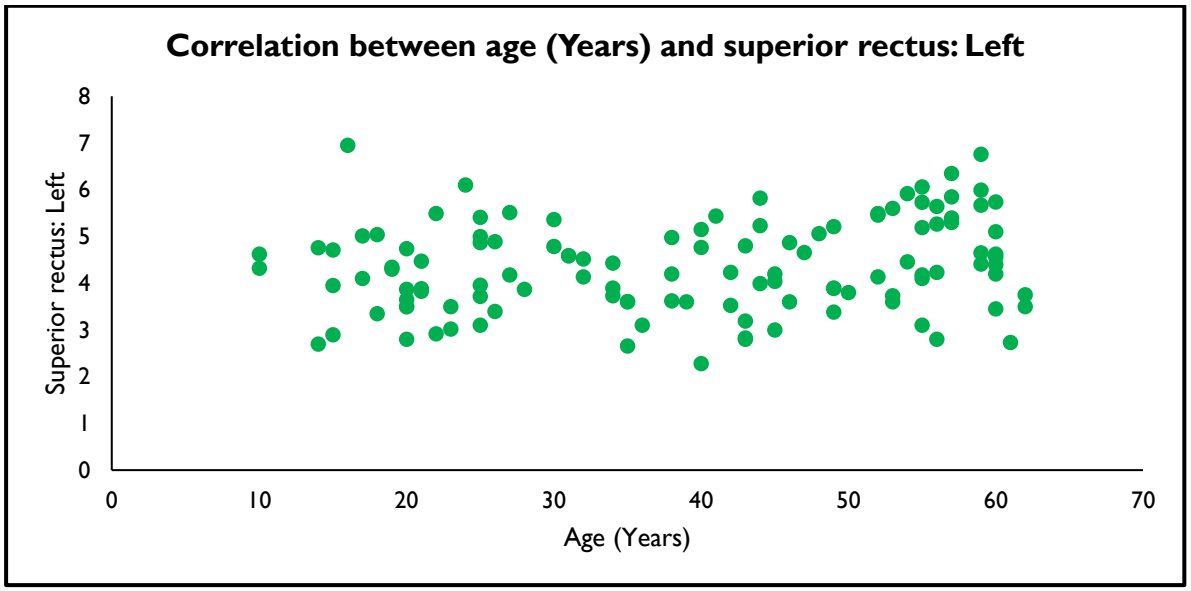

Graph 5.20 represents Correlation betweenage(years) and superior rectus:left

Table 5.9: Classification table to determine gender according to diameter of ocular muscles, and lens density

Observed		Predicted		
		Gender		Percentage Correct
		Male	Female	
Gender	Male	78	0	100
	Female	40	0	0
Overall percentage				66.1

The Binary logistic regression model was used to determine gender according to diameter of ocular muscles, and lens density. The overall accuracy of the correct prediction was 66.1%; among males it was 100%, and for females the accuracy of correct prediction was 0%. [Table – 9]

Discussion

The other research provided differ in methodology, sample size, and particular orbital parameter measurements from my study, which uses non-contrast CT to examine normative orbital measures and lens density in an Indian population. Together, the studies offer a comprehensive understanding of normative data for orbital dimensions and extraocular muscle measurements, and each one offers insightful information about the anatomy and diversity of orbital structures in various populations.

Comparison with Zhu-Hua Zhang Study-

Primarily focuses on extraocular muscle (EOM) measurements in a smaller cohort of 50 volunteers, highlighting no significant gender or side differences in most of the measurements. This contrasts with our study, which found significant gender differences in the lateral rectus and right-left side asymmetries, particularly in the inferior rectus. The size of our study (118 participants) provides more robust statistical power and allows for finer distinctions in ocular muscle diameters, lens density, and side-to-side asymmetrie. (25)

Comparison with Dr. Monu Study-

Expands on the measurements of various orbital parameters, including extraocular muscle diameters, ocular diameters, and lens density, among 90 patients. The study found a significant correlation between lens density and age, which aligns with our finding of a significant correlation between the left superior rectus and age. However, Study 2 did not find significant gender differences in most measurements, whereas our study did, especially in the lateral rectus. Study 2's focus on the interzygomatic line and other orbital parameters provides a broader scope than our study, which specifically examines the relationship between ocular muscle diameters and lens density. (18)

Comparison with Damodar Rokka Study-

From Nepal presents similar findings to Study 2, with an emphasis on orbital volume, ocular diameters, and extraocular muscle measurements. It also notes significant positive correlations between age and lens density, which is consistent with our study's finding that superior rectus measurements correlate with age. However, the study does not discuss the gender differences or right-left asymmetry in muscle diameters, which are notable findings in our research. Furthermore, the sample size (172 patients) in Study 3 strengthens its conclusions on normative orbital data, though the sample size in our study is still fairly comparable. (17)

Comparison with Vivek Gupta Study-

Which uses NCCT for evaluating orbital structures in 100 Indian patients, provides data on muscle thicknesses and orbital indices. Their findings on medial rectus (3.80–3.83 mm) and lateral rectus (3.14 mm) are somewhat similar to the measurements in our study (medical rectus: 4.50–4.52 mm; lateral rectus: 4.02–4.11 mm), but the absolute values are higher in our study. The contrast in findings between our study and Study 4 could be attributed to the methodological differences (e.g., NCCT vs. CT), the specific age groups studied, and population demographics. Additionally, Study 4's male-to-female ratio and the orbital index calculations differ slightly from the findings in your study. (20)

Overall, the comparative analysis of these studies highlights some shared findings, such as the lack of significant differences in measurements between the left and right eyes in several muscles, as well as the correlation between lens density and age. However, the differences in muscle diameters, especially lateral and inferior rectus, and the significance of gender-based variations in our study, point to potential population-specific differences. These variations may be important for the development of region-specific normative databases to aid in clinical practices and diagnosis. (25) (18) (20)

Parameter	**our Study (118 participants)**	**Zhu-Hua Zhang Study (50 participants)**	**Dr. Monu study (90 participants)**	**Damodar Rokka study (172 participants)**	**Vivek Gupta study (100 participants)**
Age Range	10–62 years	Not specified	Not specified	Not specified	Not specified
Mean Age	39.00 ± 15.45 years	Not specified	Not specified	Not specified	34.07 years
Gender Distribution	66.1% Male, 33.9% Female	50% Male, 50% Female	Not specified	Not specified	1.77 Male to Female Ratio
Sample Size	118 participants	50 participants	90 participants	172 participants	100 participants
Medial Rectus (mm)	4.50–4.52 (Right), 4.50–4.55 (Left)	3.1 ± 0.5 mm (Male), 3.1 ± 0.5 mm (Female)	0.40 ± 0.06 cm	3.67 ± 0.52 mm	3.80–3.83 mm
Lateral Rectus (mm)	4.02–4.11 (Right), 4.02–4.24 (Left)	2.2 ± 0.6 mm (Male), 2.2 ± 0.6 mm	0.32 ± 0.07 cm	3.36 ± 0.50 mm	3.14–3.46 mm

		(Female)			
Inferior Rectus (mm)	4.34–4.68 (Right), 4.26–4.37 (Left)	3.3 ± 0.8 mm (Male), 3.3 ± 0.8 mm (Female)	0.74 ± 0.11 cm	3.74 ± 0.42 mm	3.46 mm (Right), 3.36 mm (Left)
Superior Rectus (mm)	4.36–4.43 (Right), 4.23–4.38 (Left)	Not measured	0.82 ± 0.12 cm	3.87 ± 0.38 mm	3.75 mm (Right), 3.75 mm (Left)
Lens Density (HU)	77.29–77.89 (Right), 77.29–79.38 (Left)	Not specified	78.50 ± 6.92 HU	141.43 ± 16.62 HU	Not measured
Side-to-Side Asymmetry	Significant for inferior rectus ($p < 0.05$)	No significant differences	No significant differences	No significant differences	No significant differences
Gender Differences	Significant for lateral rectus (Right and Left) ($p < 0.05$)	No significant differences	Significant differences in lateral rectus (Right and Left) ($p < 0.05$)	No significant differences	No significant differences
Correlation with Age	Positive for superior rectus (Left) ($p < 0.05$)	Not specified	Positive correlation between lens density and age	Positive correlation between age, orbital volume, and ocular diameter	Not specified

Conclusion

My current study adds valuable normative data on orbital measurements, including ocular muscle diameters and lens density, specifically for an Indian population, with comparisons by age, gender, and side. The findings of significant gender-based differences in lateral rectus, as well as the right-left asymmetries in inferior rectus, offer new insights into orbital anatomy. The statistical methods used, such as the Independent sample "t" test and Pearson correlation coefficient, strengthen the study's ability to detect subtle differences that are often overlooked in smaller or less detailed studies.

The study aligns with, and in some areas extends, findings from existing literature. It corroborates the general idea that there are minimal gender-based differences in most orbital parameters but highlights the importance of gender, age, and side when interpreting orbital measurements. This is consistent with previous studies, like Study 4, which also used NCCT but focused on different age groups and smaller sample sizes.

Future Aspects

Greater Sample Size: To improve the dependability and generalization of the normative data, future research could use a larger and more varied sample size. This would facilitate the development of a more thorough knowledge of the size of the ocular muscles in various Indian population demographics.

Comparative Studies: Research on ethnic differences in ocular muscle measures can be obtained by comparing populations. This could make it easier to comprehend how these variations might impact surgical planning and clinical procedures.

Rdefined Imaging Techniques: To assess the ocular muscles more precisely, future studies could investigate the application of sophisticated imaging techniques such high-resolution MRI. This could increase the data's validity and address the drawbacks of CT-based measurements.

Clinical Applications: The normative data gathered from this study might be used to plan surgical procedures and diagnose different ocular diseases in clinical settings. In order to improve patient outcomes, future research could concentrate on creating guidelines for applying these metrics in clinical practice.

6. LIMITATIONS

• **Restricted Sample Size:** The study's fragile sample size of examined scans is one of its main shortcomings. The reliability and generalizability of the normative data acquired for ocular muscles may be impacted by a small sample size since it might not fairly represent the larger population.

Use of CT Images: Dry skull bone specimens are the optimal source of the normative data. However, the use of CT images in this investigation may have introduced measurement inconsistencies because of the presence of soft tissues and changes in imaging methodologies. This can result in inaccurate measurements of the size of the ocular muscles.

REFERENCES

[1] Schulz RA, Stein JA, Pelc NJ. How CT happened: the early development of medical computed tomography. J Med Imaging (Bellingham). 2021 Sep;8(5):052110. doi: 10.1117/1.JMI.8.5.052110. Epub 2021 Oct 29. PMID: 34729383; PMCID: PMC8555965.

[2] Al-Naser YA, Tafti D. CT Instrumentation and Physics. [Updated 2023 Nov 2]. In: StatPearls [Internet]. Treasure Island (FL): StatPearls Publishing; 2025 Jan-. Available from: https://www.ncbi.nlm.nih.gov/books/NBK597347/

[3] Curry, T. S., Dowdey, J. E., & Murry, R. E. (1990). *Christensen's physics of diagnostic radiology* (4th ed.). Lea & Febiger.

[4] Hermena S, Young M. CT-scan Image Production Procedures. [Updated 2023 Aug 8]. In: StatPearls [Internet]. Treasure Island (FL): StatPearls Publishing; 2025 Jan-. Available from: https://www.ncbi.nlm.nih.gov/books/NBK574548/

[5] Chaurasia, B. D. (2019). *BD chaurasia's human anatomy, volumes 3 & 4: Regional and applied dissection and clinical: Head and neck, and brain-neuroanatomy* (8th ed.). CBS Publishers & Distributors.

[6] Ominde, B. S., Abadom, G. E., Ikubor, J. E., Achapu, L. C., Enakpoya, P. O., & Igbigbi, P. S. (2024). Normal diameter of the optic nerve using magnetic resonance imaging: A retrospective Nigerian study. *Saudi Journal of Ophthalmology: Official Journal of the Saudi Ophthalmological Society*, *38*(1), 53–58. https://doi.org/10.4103/sjopt.sjopt_189_23

[7] Almus E, Sen Akova B, Ozer H, Fitoz S. Orbital structures in the pediatric age group: A normative assessment using magnetic resonance imaging. Eur J Radiol. 2022 Sep;154:110418. doi: 10.1016/j.ejrad.2022.110418. Epub 2022 Jun 24. PMID: 35772338.

[8] Rana, K., Juniat, V., Rayan, A., Patel, S., & Selva, D. (2022). Normative measurements of orbital structures by magnetic resonance imaging. *International Ophthalmology*, *42*(12), 3869–3875. https://doi.org/10.1007/s10792-022-02407-1

[9] Al Ajmi, E., Al Subhi, M., Al Maamari, M., Al Dhuhli, H., & Sirasanagandla, S. R. (2023). Radiologic Assessment of Orbital Dimensions among Omani Subjects: A computed tomography imaging-based study at a single tertiary centre. *Sultan Qaboos University Medical Journal*, *23*(1), 55–60. https://doi.org/10.18295/squmj.3.2022.023

[10] Rana K, Juniat V, Yong W, Patel S, Selva D. Normative orbital measurements in an Australian cohort on computed tomography. Orbit. 2023 Feb;42(1):68-72. doi: 10.1080/01676830.2022.2037143. Epub 2022 Mar 2. PMID: 35232320.

[11] Boruah, D. K., Dutta, H. K., Sarma, K., Hazarika, K., Sharma, B. K., & Goswami, A. (2021). Normative magnetic resonance imaging measurements of orbital structures in pediatric population of North-Eastern India: A retrospective cross-sectional study. *Indian Journal of Ophthalmology*, *69*(8), 2099–2105. https://doi.org/10.4103/ijo.IJO_546_21

[12] Velonakis, G., Papadopoulos, V. E., Karavasilis, E., Filippiadis, D. K., & Zouvelou, V. (2021). MRI evidence of extraocular muscle atrophy and fatty replacement in myasthenia gravis. *Neuroradiology*, *63*(9), 1531–1538. https://doi.org/10.1007/s00234-021-02753-4

[13] Gala, F. (2015). Magnetic resonance imaging of optic nerve. *The Indian Journal of Radiology & Imaging*, *25*(4), 421–438. https://doi.org/10.4103/0971-3026.169462

[14] Ozdikici, M., Bulut, E., & Agca, S. (2021). Assessment of the orbital structures using computed tomography in healthy adults. *Nigerian Journal of Clinical Practice*, *24*(4), 561–568. https://doi.org/10.4103/njcp.njcp_77_20

[15] Keene, K. R., van Vught, L., van de Velde, N. M., Ciggaar, I. A., Notting, I. C., Genders, S. W., Verschuuren, J. J. G. M., Tannemaat, M. R., Kan, H. E., & Beenakker, J.-W. M. (2021). The feasibility of quantitative MRI of extra-ocular muscles in myasthenia gravis and Graves' orbitopathy. *NMR in Biomedicine*, *34*(1), e4407. https://doi.org/10.1002/nbm.4407

[16] Yoo, R.-E., Park, S.-W., Rhim, J. H., Kim, J. E., Kim, S. C., Choe, J.-Y., Choung, H.-K., Khwarg, S. I., Kim, J.-H., Lee, J. H., Lee, B. E., & Kang, Y. (2020). CT and MR imaging findings of ocular adnexal mucosa-associated lymphoid tissue lymphoma associated with IgG4-related disease: multi-institutional case series. *International Journal of Ophthalmology*, *13*(8), 1231–1237. https://doi.org/10.18240/ijo.2020.08.08

[17] Rokka, D., Poudel, S., Kayastha, P., Suwal, S., Poudyal, S., Chhetry, S., Shrestha, S., & Karn, R. (2020). Normative measurement of orbital structures in computed tomography. *Journal of the Institute of Medicine*, *42*(3), 42–46. https://doi.org/10.3126/jiom.v42i3.37580

[18] Normative Orbital Measurements By Computed Tomography In North Indian Population - A Retrospective Study.

[19] Willett KL, Sheng M, Gorry T, Woo JH. Quality of CT Imaging of Periocular Metallic Foreign Bodies Using Artifact Reduction Software. Ophthalmic Plast Reconstr Surg. 2019 Sep/Oct;35(5):438-443. doi: 10.1097/IOP.0000000000001295. PMID: 30688722.

[20] Gupta, V., Prabhakar, A., Yadav, M., & Khandelwal, N. (2019). Computed tomography imaging-based normative orbital measurement in Indian population. *Indian Journal of Ophthalmology*, *67*(5), 659. https://doi.org/10.4103/ijo.ijo_1187_18

[21] *MeasurementoftheOrbitalSoftTissueVolumeinChineseAdults Based on Three-Dimensional CT Reconstruction*. (n.d.).

[22] Xu, L., Li, L., Xie, C., Guan, M., & Xue, Y. (2017). Thickness of extraocular muscle and orbital fat in MRI predicts response to glucocorticoid therapy in Graves' ophthalmopathy. *International Journal of Endocrinology*, *2017*, 3196059. https://doi.org/10.1155/2017/3196059

[23] Khademi, Z., & Bayat, P. (2016). Computed tomographic measurements of orbital entrance dimensions in relation to age and gender in a sample of healthy Iranian population. *Journal of Current Ophthalmology*, *28*(2), 81–84. https://doi.org/10.1016/j.joco.2016.03.002

[24] Pitceathly, R. D. S., Morrow, J. M., Sinclair, C. D. J., Woodward, C., Sweeney, M. G., Rahman, S., Plant, G. T., Ali, N., Bremner, F., Davagnanam, I., Yousry, T. A., Hanna, M. G., & Thornton, J. S. (2016). Extra-ocular muscle MRI in genetically-defined mitochondrial disease. *European Radiology*, *26*(1), 130–137. https://doi.org/10.1007/s00330-015-3801-5

[25] Zhang, Z.-H., Chen, Y., Wang, Y., Meng, W., Fang, H.-Y., Xu, D.-D., & Jin, Z.-Y. (2013). Normative measurements of extraocular musculature by multislice computed tomography. *Chung-Kuo i Hsueh k'o Hsueh Tsa Chih [Chinese Medical Sciences Journal]*, *27*(4), 232–236. https://doi.org/10.1016/s1001-9294(13)60007-3

[26] Dhanwate, A. D., Associate Professor, Department of Anatomy, Government Medical College, Akola, Maharashtra, India (Former- Assistant Professor, Department of Anatomy, Government Medical College, Aurangabad, Maharashtra, India)., Gaikwad, M. D., & Lecturer, Department of Pathology, CSMSS Ayurved College, Aurangabad, Maharashtra, India. (2016). Morphometric analysis of orbit in Indian skulls and comparison with international studies. International Journal of Anatomy and Research, 4(4.1), 2896–2901. https://doi.org/10.16965/ijar.2016.363

[27] Li R, Xia S, Wang J, Sun F, Qi J. [MRI study of the thickness and width of the extraocular muscles in normal subjects]. Zhonghua Yan Ke Za Zhi. 2015 Jun;51(6):434-8. Chinese. PMID: 26310117